INTERNATIONAL JOURNAL OF HYDROGEN ENERGY XXX (2016) 1–7

Available online at www.sciencedirect.com

ScienceDirect

journal homepage: www.elsevier.com/locate/he

# Synthesis of a $MoS_{2(1-x)}Se_{2x}$ ternary alloy on carbon nanofibers as the high efficient water splitting electrocatalyst

*Hui Yang, Ting Zhang, Han Zhu, Ming Zhang, WeiWei Wu, MingLiang Du* *

*College of Materials and Textiles, Zhejiang Sci-Tech University, Hangzhou, 310018, PR China*

ARTICLE INFO

*Article history:*
Received 19 July 2016
Received in revised form
9 October 2016
Accepted 14 October 2016
Available online xxx

*Keywords:*
$MoS_{2(1-x)}Se_{2x}$
Ternary alloy
Carbon nanofiber
Hydrogen evolution reaction
Catalyst

ABSTRACT

Binary transition metal dichalcogenides (TMDs) usually exhibit high hydrogen evolution reaction (HER) activities; however, the facile and efficient synthesis of ternary TMDs alloys remains a challenge. In this study, we reported an efficient method of synthesis for a $MoS_{2(1-x)}Se_{2x}$ ternary alloy in a CVD system, and carbon nanofibers serve as the substrate. The $MoS_{2(1-x)}Se_{2x}$/CNFs hybrids were directly used as hydrogen evolution cathodes and exhibit lower onset potentials and excellent durability, suggesting they have significantly enhanced catalytic activity and could serve as effective and promising catalysts for the HER.



## Introduction

As a clean and sustainable energy carrier, hydrogen is considered to be a promising and appealing solution to take the place of fossil fuels. Among the hydrogen production methods, the hydrogen evolution reaction (HER) is an efficient electrochemical process to produce hydrogen by water splitting [1,2]. Conventionally, the platinum group metals (e.g., Pt) are demonstrated to be the most effective electrocatalysts for the hydrogen evolution reaction. However, because of the rarity and high cost of the platinum group metals, their extensive application is essentially throttled [2,3]. Extensive investigations about inexpensive alternatives with high electrocatalytic activity have found that layered transition metal dichalcogenides (TMDs) are especially attractive. Because of the special layered structures, weak van der Waals forces between molecular layers, and strong chemical bonding within the layers, TMDs have demonstrated numerous applications in fields such as water splitting, optoelectronics, and nanoelectronics [4].

Recently, numerous studies have been committed to improve TMDs' electrocatalytic performance [5–9]. As is well known, there are three major approaches to optimize their HER activities: (1) increasing the number of active sites of the catalyst, (2) improving the electrical conductivity of the catalyst, and (3) improving the catalytic effects of the active sites [3]. Cui et al. have fabricated layered $MoSe_2$ and $WSe_2$ vertically oriented on curved and rough surfaces that exhibited a significantly enhanced HER activity and an extremely high

* *Corresponding author*. Fax: +86 571 86843255.
E-mail address: du@zstu.edu.cn (M. Du).

http://dx.doi.org/10.1016/j.ijhydene.2016.10.075



Please cite this article in press as: Yang H, et al., Synthesis of a $MoS_{2(1-x)}Se_{2x}$ ternary alloy on carbon nanofibers as the high efficient water splitting electrocatalyst, International Journal of Hydrogen Energy (2016), http://dx.doi.org/10.1016/j.ijhydene.2016.10.075

stability because such oriented structures possess maximally exposed active edges [6]. Previously, we reported layered $MoSe_2$ grown on carbon nanofibers (CNFs), and the obtained nanomaterials exhibited substantially improved catalytic activity because of the large surface area and high conductivity of CNFs.

As is well known, carbonaceous materials, such as graphene, carbon nanotubes and carbon nanofibers, can substantially improve the conductivity of catalysts. Moreover, numerous studies indicate that cation dopants (Ni, Co and etc.) in the layered TMDs could optimize and significantly increase the catalytic activities [10–16]. Considering the similarities in atomic structure and properties of the TMDs' family members ($MX_2$: M = Mo, W; X = S, Se, Te), it is probable to create a multicomponent alloy system without phase separation by the doping of TMDs with another chalcogen, and the introduction of another chalcogen into TMDs could improve the HER performance [17–20]. Sampath et al. have investigated the introduction of Se substitution into the $MoS_2$ lattice, and the results suggested that the catalytic activity of sulfoselenides could be optimized by tuning the composition [21]. Bin Xiang et al. have reported one dimensional single-crystal $MoS_{2(1-x)}Se_{2x}$ nanobelts with controllable Se and S content, indicating that the introduction of Se into $MoS_2$ would change the electronic structures of the $MoS_{2(1-x)}Se_{2x}$ nanobelts and significantly improve the HER electrocatalytic activity [22].

In this study, on the basis of our previous work, we report an efficient method of synthesis for $MoS_{2(1-x)}Se_{2x}$ in a chemical vapor deposition (CVD) system with CNFs serving as substrate. Firstly, electrospinning polyacrylonitrile (PAN) mats were synthesized and then carbonized to CNFs. Subsequently, the rapid sulfurization and selenization of $MoO_3$ were performed in a CVD system to attain the $MoS_{2(1-x)}Se_{2x}$/CNFs hybrids. The $MoS_{2(1-x)}Se_{2x}$/CNFs hybrids were directly employed as the working electrode in a typical three-electrode system and exhibited excellent electrocatalytic activity and stability.

## Experiments

### Synthesis of $MoS_{2(1-x)}Se_{2x}$/CNFs hybrids

$MoS_{2(1-x)}Se_{2x}$/CNFs hybrids were synthesized in a quartz tube furnace by the chemical vapor deposition (CVD) method. A ceramic boat with carbon nanofibers was placed in the downstream of the furnace with the temperature at approximately 750 °C. The S powder and Se powder were put into the first and second heating zones, respectively; the boat with the $MoO_3$ powder was placed between the Se and the CNFs' boat. The loadings of the S powder and Se powder were approximately 0.4 g and 0.2 g. Before the growth, argon gas was flowed through the tube at a flow rate of 70 sccm to remove residual oxygen. Then, we heated the furnace up to 750 °C in an hour and maintained the reaction temperature for an hour. When the temperature of the furnace reached 400 °C, the first heating zone (S powder) was rapidly raised to 150 °C. This was followed by a natural cool-down period during which Ar gas was kept flowing at a rate of 70 sccm to transport sulfur and selenium to the substrate.

### Instruments

The sample morphology was observed using a JSM-2100 transmission electron microscope (JEOL, Japan) at an acceleration voltage of 200 kV and a JSM-6700 field-emission scanning electron microscope (JEOL, Japan) at an acceleration voltage of 3 kV. The X-ray photoelectron spectra of the samples were obtained by an X-ray photoelectron spectrometer (Kratos Axis Ultra DLD) with an Al (mono) Kα source (1486.6 eV). The Al Kα source was operated at 15 kV and 10 mA. X-ray diffraction (XRD) patterns were recorded using a Bruker AXS D8 DISCOVER X-ray diffractometer with Cu Kα radiation (λ = 1.5406 Å) at a scanning rate of 0.02 2θ $s^{-1}$ in a 2θ range of 10–80°. The Raman spectra of all of the samples were obtained by a Renishaw in Via Raman microscope (LabRAM HR800) using a 532 nm laser excitation source. The excitation light intensity in front of the objective was 10 mW with a spectral collection time of 1 s. The integration time for the measurements was set to 10 s. High-angle annular dark field scanning TEM (HAADF-STEM) images, STEM mapping and line-scan energy dispersive X-ray spectroscopy (EDX) spectra were recorded by a STEM (Tecnai G2 F30S-Twin, Philips-FEI) at an acceleration voltage of 300 kV.

### Electrochemical characterization

The electrochemical measurements of all of samples were conducted in a standard three-electrode system in a 0.5 M $H_2SO_4$ solution (deaerated by Ar for 30 min). The $MoS_{2(1-x)}Se_{2x}$/CNFs hybrid, platinum mesh electrode and saturated calomel electrode served as the working, counter and reference electrodes, respectively. The HER activity was evaluated by linear sweep voltammetry, which was recorded using a CHI660E workstation (Shanghai Chenhua, Shanghai) at a scan rate of 1 mV/s. The polarization curves were obtained after iR-compensation. In all of the measurements, a Hg/$Hg_2Cl_2$ electrode was used as the reference, and the potential values were corrected to the reverse hydrogen electrode (RHE).

## Results and discussion

In the study, the $MoS_{2(1-x)}Se_{2x}$ alloy nanostructures were synthesized on the CNFs substrate in a home-built quartz tube furnace by the CVD method. The precursors were converted to the vapor phase at a high temperature and transported to the substrate by a carrier gas of argon. In the process, $MoS_{2(1-x)}$-$Se_{2x}$ was obtained by the rapid sulfurization and selenization of $MoO_3$. Herein, the morphology of the as-grown $MoS_{2(1-x)}$-$Se_{2x}$ nanoflakes is dominated by the hexagonal layer. The SEM images of the low-density $MoS_{2(1-x)}Se_{2x}$/CNFs (denoted as $MoS_{2(1-x)}Se_{2x}$ (LD)/CNFs) hybrid and the high-density $MoS_{2(1-x)}Se_{2x}$/CNFs (denoted as $MoS_{2(1-x)}Se_{2x}$ (HD)/CNFs) hybrid are shown in Fig. 1. As illustrated in Fig. 1a and c, the CNFs are a three-dimensional substrate with each fiber approximately 0.2 μm in diameter, and the $MoS_{2(1-x)}Se_{2x}$ nanoflakes were radially grown onto the CNFs. Fig. 1b presents the nanoflakes irregularly stacked together with several layers, and the lengths of the hexagonal nanoflakes are approximately 1 μm. For the $MoS_{2(1-x)}Se_{2x}$ (HD)/CNFs hybrid,

Please cite this article in press as: Yang H, et al., Synthesis of a $MoS_{2(1-x)}Se_{2x}$ ternary alloy on carbon nanofibers as the high efficient water splitting electrocatalyst, International Journal of Hydrogen Energy (2016), http://dx.doi.org/10.1016/j.ijhydene.2016.10.075

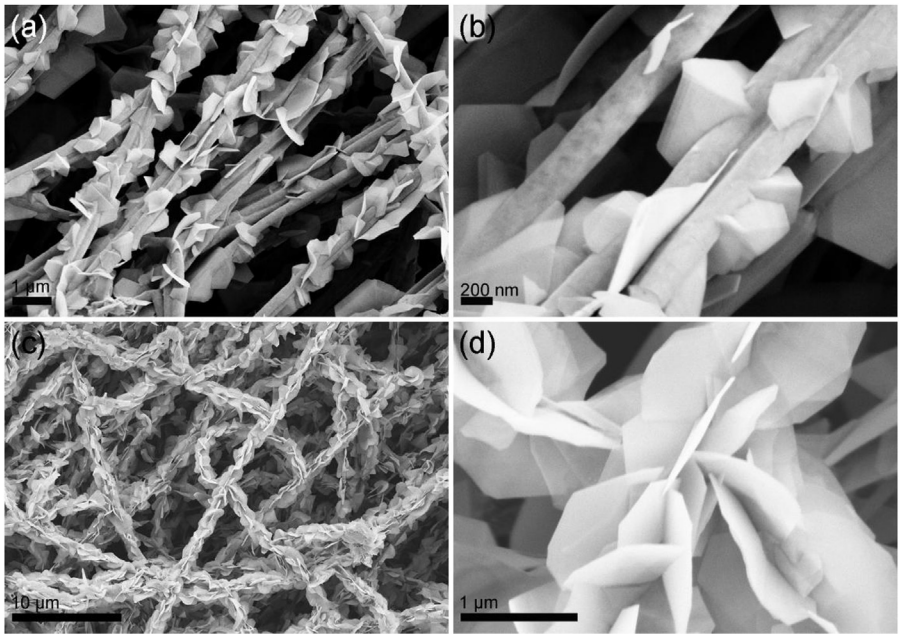


**Fig. 1 – FE-SEM images of (a) and (b) the low-density $MoS_{2(1-x)}Se_{2x}$/CNFs hybrid, and (c) and (d) the high-density $MoS_{2(1-x)}Se_{2x}$/CNFs hybrid.**

the $MoS_{2(1-x)}Se_{2x}$ nanoflakes grew vertically on the CNFs (as shown in Fig. 1c), and the surface of CNFs is uniformly covered with nanoflakes. In Fig. 1d, the lengths of the hexagonal nanoflakes are also approximately 1 μm. Moreover, we can observe that the $MoS_{2(1-x)}Se_{2x}$ nanoflakes were a hexagonal layer in structure, not a pure hexagon, but a structure more like a triangle that intercepted at the three corners. Such edge-terminated nanoflakes were expected to be highly efficient HER catalysts because they expose the edge sites maximally [5].

Fig. 2a presents the obtained $MoS_{2(1-x)}Se_{2x}$ (LD) nanoflakes wrapping the surface of the CNFs, and herein, the nanoflakes are of irregular shapes. Moreover, we can observe the thickness of each nanoflake is several nanometers. The inset of Fig. 2a presents a high-resolution transmission electron microscope (HRTEM) image of a typical nanoflake, indicating the high-quality crystallinity with the lattice fringes of 0.25 nm, which is in good agreement with (102) lattice planes. The HRTEM image of a typical nanoflake is shown in Fig. 2b and demonstrates that the nanoflake is not a pure hexagon but a structure more like a triangle with three corners intercepted, in good agreement with the SEM results. As presented in the inset of Fig. 2b, the selected area electron diffraction (SAED) pattern shows six-fold symmetry diffraction spots, further

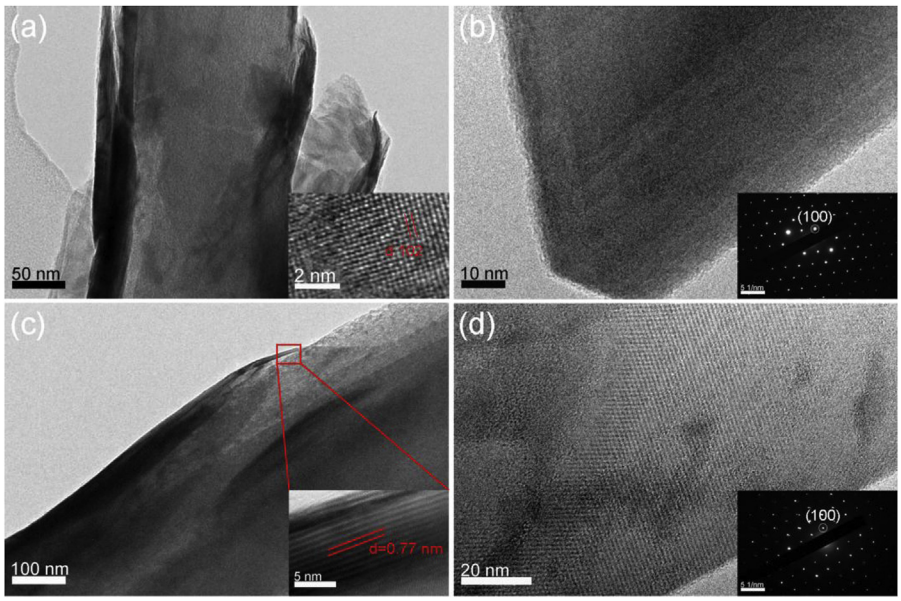


**Fig. 2 – TEM images of (a) the $MoS_{2(1-x)}Se_{2x}$ (LD)/CNFs hybrid and (b) an HRTEM image of a typical $MoS_{2(1-x)}Se_{2x}$ nanoflake; (c) the $MoS_{2(1-x)}Se_{2x}$ (HD)/CNFs hybrid and (d) an HRTEM image of a typical $MoS_{2(1-x)}Se_{2x}$ nanoflake.**

Please cite this article in press as: Yang H, et al., Synthesis of a $MoS_{2(1-x)}Se_{2x}$ ternary alloy on carbon nanofibers as the high efficient water splitting electrocatalyst, International Journal of Hydrogen Energy (2016), http://dx.doi.org/10.1016/j.ijhydene.2016.10.075

confirming the single-crystalline nature of the nanoflakes. In Fig. 2c, the $MoS_{2(1-x)}Se_{2x}$ (HD) nanoflakes stuck to the surface of the CNFs. In the inset, the corresponding selected area image is shown, revealing that the nanoflake consists of many layers, and the space between the layers is approximately 0.77 nm. As shown in Fig. 2d and the inset, we can observe a fringe in the nanoflake, and the SAED pattern shows six-fold symmetry diffraction spots, also confirming the single-crystalline nature of the nanoflakes. To unambiguously determine the distribution of elements, we employed elemental mapping by scanning transmission electron microscopy (STEM), and the high-resolution EDS elemental mapping images are shown in Fig. 3a and b. This confirms the homogeneous distribution of Mo, S and Se elements across the substrate, and a high spatial correlation is presented over the entire area mapped, demonstrating the single-phase construction of S and Se without the phase separation of $MoS_2$ and $MoSe_2$.

To further probe the chemical composition of the $MoS_{2(1-x)}Se_{2x}$/CNFs hybrids, XPS characterizations were conducted. Fig. 4a–d presents the survey, and Mo 3d, S 2p, and Se 3d high-resolution spectra of the as-grown hybrid. As shown in Fig. 4a, the result indicates that a composition of C, Mo, S, and Se exists in the hybrid, in good accordance with the mapping result. The intensity of the C 1s is the strongest among all of peaks, revealing that the carbonaceous material is dominant in the hybrid, and it could improve the conductivity of the $MoS_{2(1-x)}Se_{2x}$ semiconductor. In Fig. 4b, the two clear peaks located at 232.5 eV and 229.4 eV are the characteristic Mo $3d_{3/2}$ and Mo $3d_{5/2}$ peaks, respectively, and are consistent with values from $MoS_2$ and $MoSe_2$ systems [23–25]. The Mo $3d_{5/2}$ peak located at 229.4 eV is the characteristic peak of the Mo +4 oxidation state in the hexagonal 2H phase [2,26]. The peaks for S 2p between 158 eV and 170 eV can be deconvoluted into four peaks (Fig. 4c). The S $2p_{1/2}$ and $2p_{3/2}$ peaks emerge with binding energies of 163.7 eV and 162.4 eV, respectively [21,22,25]. They are in agreement with the binding energies of the corresponding peaks in $MoS_2$, demonstrating the existence of Mo–S bonding instead of elemental S [27,28]. Whereas the other two obvious peaks located at approximately 167.0 eV and 161.2 eV are assigned to Se $3p_{1/2}$ and $3p_{3/2}$, respectively [3,25,29]. The peaks at approximately 55.7 eV and 54.9 eV are attributed to Se $3d_{3/2}$ and $3d_{5/2}$, respectively, as shown in Fig. 4d.

XRD and Raman spectroscopy were utilized to investigate the nanostructure information of the $MoS_{2(1-x)}Se_{2x}$/CNFs hybrid. The diffraction peaks of the samples in the XRD pattern reveal the good purity of the products, as shown in Fig. 5a. The good crystallinity of the samples is likely advantageous for the catalytic activity and stability [20]. The broad diffraction peak at a 2θ value of 23.3° is attributed to the diffraction plane of (002) for graphitic carbon. The characteristic diffraction peaks in the case of $MoSe_2$/CNFs located at 2θ value of 13.60°, 31.71°, 37.35°, and 57.09° correspond to the (002), (100), (103), and (110) diffraction planes, respectively. Moreover, the characteristic diffraction peaks of the $MoS_{0.44}Se_{1.56}$/CNFs slightly shift to higher angles, and such a slight displacement is expected as S has a smaller ionic radius than Se [3,30,31], which indicates that the mixing of Se and S is on the atomic scale.

Raman spectroscopy was used to characterize the composition-dependent vibration modes of the $MoS_{2(1-x)}Se_{2x}$/CNFs hybrid, as presented in Fig. 5b. As is well known, two kinds of characteristic Raman vibrational modes can be gained in 2D metal dichalcogenides: the in-plane vibrational mode (E mode) and the out-plane vibrational mode (A mode). In the case of the ternary alloy $MoS_{2(1-x)}Se_{2x}$, the vibrational modes can be classified into two sets of composition-dependent modes: Mo–Se-related modes at low frequency (200–300 $cm^{-1}$) and Mo–S-related modes at high frequency (350–410 $cm^{-1}$) [2]. For the low frequency modes of the $MoS_{2(1-x)}Se_{2x}$/CNFs hybrid, two identifiable peaks can be found at approximately 233.54 $cm^{-1}$ and 248.90 $cm^{-1}$, corresponding to the $MoSe_2$-like $A_{1g}$ and $E_{2g}$, respectively. The intensities of the $MoS_2$-like vibration modes are less than those of $MoSe_2$, and the peaks located at approximately 380.88 $cm^{-1}$ and 441.23 $cm^{-1}$ can be assigned to the $MoS_2$-like $E_{2g}$ and $A_{1g}$, respectively. Moreover, for the high frequency modes of the hybrid, two sharp peaks at 1334.29 $cm^{-1}$ and 1584.78 $cm^{-1}$ can be ascribed to the D and G bands of the carbon nanofibers substrate.

Based on the above discussion, the $MoS_{2(1-x)}Se_{2x}$ nanoflakes with a hexagonal morphology were successfully prepared on the surface of the CNFs. The characterizations reveal

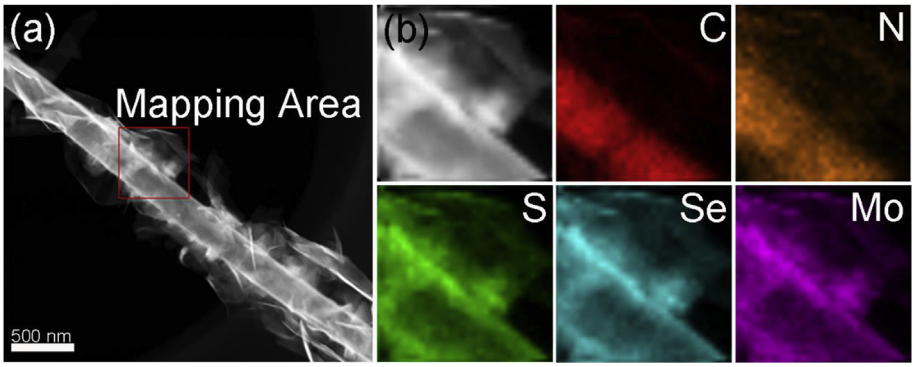


**Fig. 3 – (a) HAADF STEM image of the $MoS_{2(1-x)}Se_{2x}$/CNFs hybrids, and (b) the corresponding elemental distribution obtained from the mapping area in (a).**

Please cite this article in press as: Yang H, et al., Synthesis of a $MoS_{2(1-x)}Se_{2x}$ ternary alloy on carbon nanofibers as the high efficient water splitting electrocatalyst, International Journal of Hydrogen Energy (2016), http://dx.doi.org/10.1016/j.ijhydene.2016.10.075

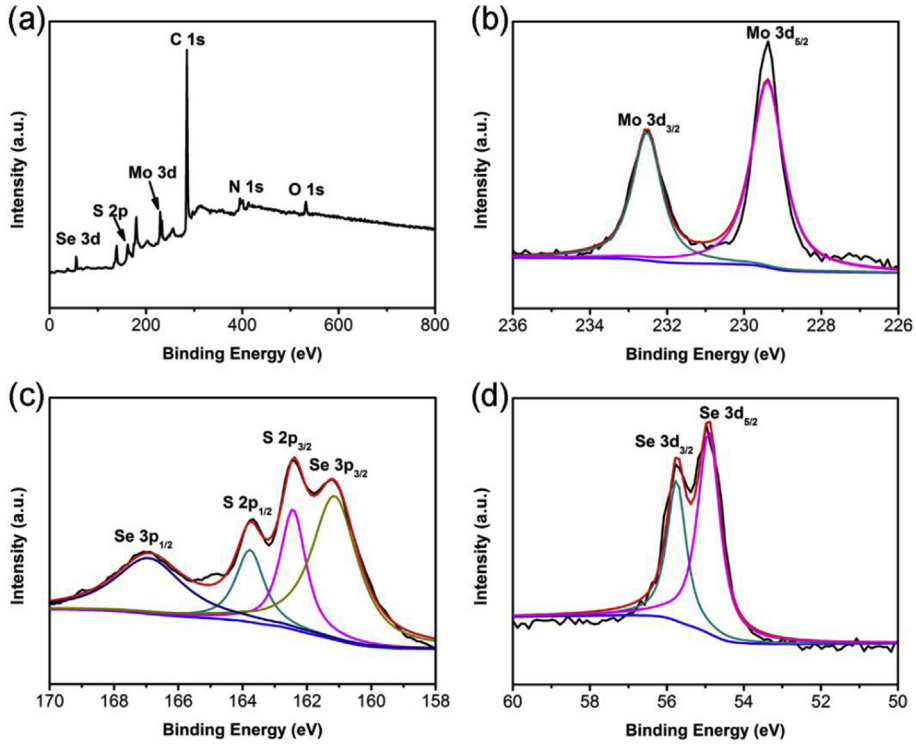


**Fig. 4 – XPS spectra of (a) the survey, (b) Mo 3d, (c) S 2p, and (d) Se 3d of the $MoS_{2(1-x)}Se_{2x}$/CNFs hybrid.**

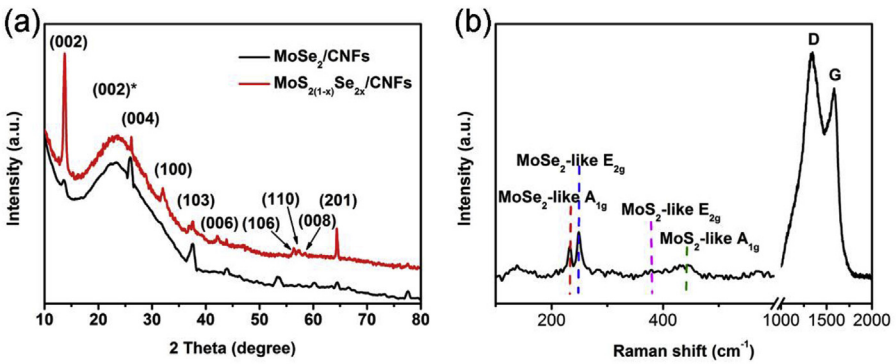


**Fig. 5 – (a) XRD patterns of the $MoSe_2$/CNFs hybrid (black) and the $MoS_{2(1-x)}Se_{2x}$/CNFs hybrid (red); (b) the Raman spectrum of $MoS_{2(1-x)}Se_{2x}$/CNFs hybrid. (For interpretation of the references to colour in this figure legend, the reader is referred to the web version of this article.)**

the good crystallinity of the $MoS_{2(1-x)}Se_{2x}$ nanoflakes and their maximally exposed edge sites, which are critical for HER catalysts. A typical three-electrode system and 0.5 M $H_2SO_4$ (aq) was utilized to evaluate the HER activity. The hybrid was directly assembled as the working electrode. The platinum mesh electrode and the saturated calomel electrode were used as the counter electrode and the reference electrode, respectively. The polarization curves reveal that the $MoS_{2(1-x)}Se_{2x}$ (HD)/CNFs hybrid exhibited the smallest onset potential of approximately 54 mV *vs.* RHE, as shown in Fig. 6a. Significantly, in the case of the $MoS_{2(1-x)}Se_{2x}$ (LD)/CNFs hybrid, the onset potential is substantially higher than that of the $MoS_{2(1-x)}Se_{2x}$ (HD)/CNFs hybrid (approximately 104 mV *vs.* RHE). Moreover, the onset potential of the $MoSe_2$/CNFs hybrid is approximately 137 mV *vs.* RHE. And the $MoS_2$/CNFs hybrid exhibits higher onset potential of 167 mV *vs.* RHE. Interestingly, the $MoS_{2(1-x)}Se_{2x}$ (HD)/CNFs hybrid demonstrated the best activity for the HER with an overpotential of 150 mV (*vs.* RHE) at a current density of 10 mA/cm$^2$ and the $MoS_{2(1-x)}Se_{2x}$ (LD)/CNFs hybrid possesses a higher overpotential of 272 mV (*vs.* RHE), which is less than that of the $MoSe_2$/CNFs hybrid (approximately 345 mV *vs.* RHE) and the $MoS_2$/CNFs hybrid (approximately 281 mV *vs.* RHE).

The Tafel slope is another critical factor for the HER, and an inherent property of the rate-determining step in the HER. The slopes were obtained by the fitting of the linear regions, according to the Tafel equation: $\eta = b \log j + a$, where $\eta$ is the overpotential, b is the Tafel slope, and $j$ is the current density. As shown in Fig. 6b, the $MoSe_2$/CNFs hybrid exhibits the largest Tafel slope (166 mV/dec), and the value for the

Please cite this article in press as: Yang H, et al., Synthesis of a $MoS_{2(1-x)}Se_{2x}$ ternary alloy on carbon nanofibers as the high efficient water splitting electrocatalyst, International Journal of Hydrogen Energy (2016), http://dx.doi.org/10.1016/j.ijhydene.2016.10.075

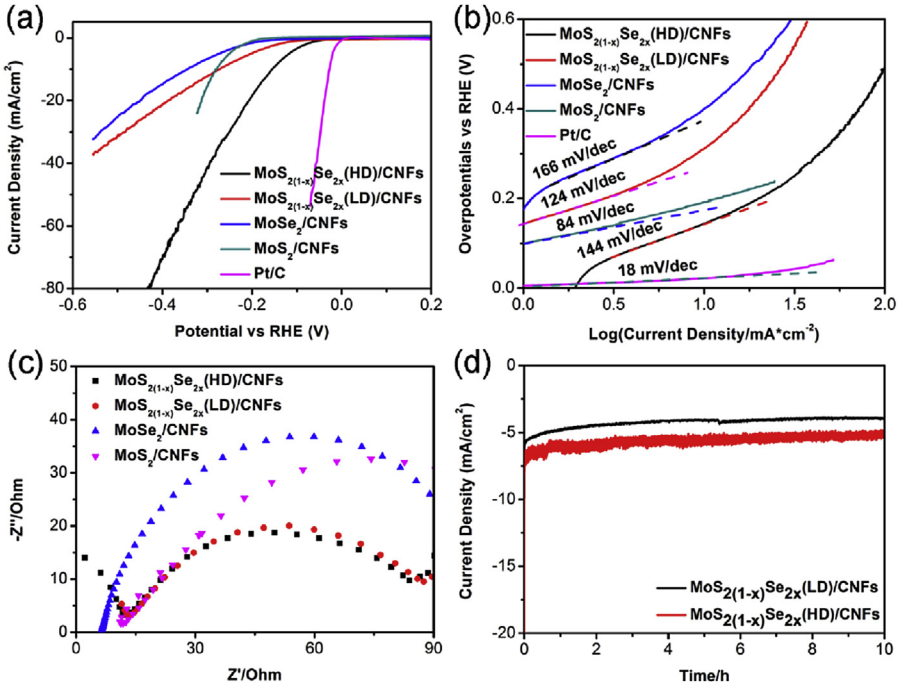


**Fig. 6 – (a) Polarization curves obtained for $MoSe_2$/CNFs, $MoS_2$/CNFs, $MoS_{2(1-x)}Se_{2x}$ (LD)/CNFs, $MoS_{2(1-x)}Se_{2x}$ (HD)/CNFs, and Pt/C as indicated, (b) the corresponding Tafel plots and (c) the electrochemical impedance spectra of $MoSe_2$/CNFs, $MoS_2$/CNFs, $MoS_{2(1-x)}Se_{2x}$ (LD)/CNFs and $MoS_{2(1-x)}Se_{2x}$ (HD)/CNFs, and (d) the time dependence of the current density under a static overpotential of −0.5 V.**

$MoS_{2(1-x)}Se_{2x}$ (HD)/CNFs hybrid is 144 mV/dec, which suggests it follows the Volmer-Heyrovsky or the Volmer-Tafel process with the Volmer reaction as the rate-determining step. Strangely, an abnormal phenomenon occurred with the $MoS_{2(1-x)}Se_{2x}$ (LD)/CNFs hybrid yielding a value of the Tafel slope as 124 mV/dec, which is substantially less than that of the $MoS_{2(1-x)}Se_{2x}$ (HD)/CNFs hybrid. Generally, a smaller Tafel slope means an improvement in the HER rate at a moderate increase of overpotential [3,22,32,33]. Besides the HER catalysis active sites, the enhanced charge transfer kinetics also contribute to the improved HER efficiency of a catalysts [3]. We evaluated the Ac impedance at an overpotential of −300 mV (as shown in Fig. 6c). The ternary alloy hybrid exhibits a smaller charge transfer impendence at range of 70–80 Ohm than that of the $MoSe_2$/CNFs hybrid (~120 Ohm) and $MoS_2$/CNFs hybrid (~150 Ohm), suggesting faster HER kinetics with $MoS_{2(1-x)}Se_{2x}$/CNFs.

The durability of the catalysts is another important property for the HER. The time dependence of the current density was investigated at an overpotential of −0.5 V for 36,000 s. As shown in Fig. 6d, the current density of the ternary alloy hybrid remained stable for 10 h, and only a slight decrease was observed, indicating the excellent electrocatalytic durability of the $MoS_{2(1-x)}Se_{2x}$/CNFs hybrids.

In the present investigations, we investigated and determined the elements by XPS characterizations. We calculated the ratio of Se/S by the formula: $Se/S = (I_{Se}{}^*F_S)/(I_S{}^*F_{Se})$, where $I_{Se}$ and $I_S$ are the areas under the peaks of Se $3p_{3/2}$ and S $2p_{3/2}$, respectively; $F_{Se}$ and $F_S$ represent the relative symmetric factors (R.S.F) for Se $3p_{3/2}$ (0.4453) and S $2p_{3/2}$ (0.8493) respectively [21,22]. In the case of $MoS_{2(1-x)}Se_{2x}$(HD)/CNFs and $MoS_{2(1-x)}$-$Se_{2x}$(LD)/CNFs, the x is determined as 0.78 and 0.64, respectively.

In earlier theoretical calculations, the results revealed that the $\Delta G_H$ of hydrogen adsorption for Mo–S edges is 80 meV and that of Mo–Se edges is −140 meV [22,34,35]. It reaches the thermoneutral with the free energy of adsorbed atomic hydrogen to $\Delta G_H \approx 0$. With the introduction of Se into $MoS_2$ lattice, the oxidation state of Mo would be changed. The increasing of Se content, the energy barrier in the chemical reaction would decrease, resulting lower hydrogen adsorption energy and higher HER performance [22]. As a consequence, the $MoS_{2(1-x)}Se_{2x}$(HD)/CNFs and $MoS_{2(1-x)}Se_{2x}$(LD)/CNFs catalysts exhibit much higher electrochemical activity compared with $MoSe_2$/CNFs and $MoS_2$/CNFs.

## Conclusions

In summary, the hexagonal layered $MoS_{2(1-x)}Se_{2x}$ nanoflakes were successfully grown onto carbon nanofibers by the CVD method. The ternary alloy nanoflakes with an abundance of exposed active edge sites were uniformly stacked on the surface of the CNFs. The as-prepared $MoS_{2(1-x)}Se_{2x}$/CNFs hybrids were directly used as hydrogen evolution cathodes, and all of the samples exhibited a lower onset potential, a higher current density, and excellent durability, suggesting $MoS_{2(1-x)}Se_{2x}$/CNFs hybrid has significantly enhanced catalytic activity and could serve as an effective and promising catalyst for the HER.

Please cite this article in press as: Yang H, et al., Synthesis of a $MoS_{2(1-x)}Se_{2x}$ ternary alloy on carbon nanofibers as the high efficient water splitting electrocatalyst, International Journal of Hydrogen Energy (2016), http://dx.doi.org/10.1016/j.ijhydene.2016.10.075

## Acknowledgments

This study was supported by the National Natural Science Foundation of China (NSFC) (Grant number. 51373154, 51573166), the Program for Innovative Research Team of Zhejiang Sci-Tech University and the 521 Talent Project of Zhejiang Sci-Tech University.

## REFERENCES

[1] Morales-Guio CG, Stern LA, Hu X. Nanostructured hydrotreating catalysts for electrochemical hydrogen evolution. Chem Soc Rev 2014;43:6555–69.
[2] Gong Q, Cheng L, Liu C, Zhang M, Feng Q, Ye H, et al. Ultrathin $MoS_{2(1-x)}Se_{2x}$ alloy nanoflakes for electrocatalytic hydrogen evolution reaction. ACS Catal 2015;5:2213–9.
[3] Xu C, Peng S, Tan C, Ang H, Tan H, Zhang H, et al. Ultrathin S-doped $MoSe_2$ nanosheets for efficient hydrogen evolution. J Mater Chem A 2014;2:5597–601.
[4] Feng Q, Mao N, Wu J, Xu H, Wang C, Zhang J, et al. Growth of $MoS_{2(1-x)}Se_{2x}$ ($x = 0.41–1.00$) monolayer alloys with controlled morphology by physical vapor deposition. ACS Nano 2015;9:7450–5.
[5] Kong D, Wang H, Cha J, Pasta M, Koski K, Yao J, et al. Synthesis of $MoS_2$ and $MoSe_2$ films with vertically aligned layers. Nano Lett 2013;13:1341–7.
[6] Wang H, Kong D, Johanes P, Cha J, Zheng G, Yan K, et al. $MoSe_2$ and $WSe_2$ nanofilms with vertically aligned molecular layers on curved and rough surfaces. Nano Lett 2013;13:3426–33.
[7] Wu Z, Fang B, Wang Z, Wang C, Liu Z, Liu F, et al. $MoS_2$ nanosheets: a designed structure with high active site density for the hydrogen evolution reaction. ACS Catal 2013;3:2101–7.
[8] Kim J, Byun S, Smith A, Yu J, Huang J. Enhanced electrocatalytic properties of transition-metal dichalcogenides sheets by spontaneous gold nanoparticle decoration. J Phys Chem Lett 2013;4:1227–32.
[9] Chhowalla M, Shin H, Eda G, Li L, Loh K, Zhang H. The chemistry of two-dimensional layered transition metal dichalcogenide nanosheets. Nat Chem 2013;5:263–75.
[10] Merki D, Vrubel H, Rovelli L, Fierro S, Hu X. Fe, Co, and Ni ions promote the catalytic activity of amorphous molybdenum sulfide films for hydrogen evolution. Chem Sci 2012;3:2515–25.
[11] Lv X, She G, Zhou S, Li Y. Highly efficient electrocatalytic hydrogen production by nickel promoted molybdenum sulfide microspheres catalysts. RSC Adv 2013;3:21231–6.
[12] Li J, Tang W, Yang H, Dong Z, Huang J, Li S, et al. Enhanced-electrocatalytic activity of $Ni_{1-x}Fe_x$ alloy supported on polyethyleneimine functionalized $MoS_2$ nanosheets for hydrazine oxidation. RSC Adv 2014;4:1988–95.
[13] Zhou T, Yin H, Liu Y, Chai Y, Zhang J, Liu C. Synthesis, characterization and HDS activity of carbon-containing Ni–Mo sulfide nano-spheres. Catal Lett 2010;134:343–50.
[14] Alvarez L, Berhault G, Alonso-Nunez G. Unsupported NiMo sulfide catalysts obtained from nickel/ammonium and nickel/tetraalkylammonium thiomolybdates: synthesis and application in the hydrodesulfurization of dibenzothiophene. Catal Lett 2008;125:35–45.
[15] Liu B, Chai Y, Liu Y, Wang Y, Liu Y, Liu C. A simple method for preparation of presulfided eggshell CoMoS/$\gamma$-$Al_2O_3$ catalysts for hydrodesulfurization of dibenzothiophene. Fuel 2012;95:457–63.
[16] Okamoto Y, Hioka K, Arakawa K, Fujikawa T, Ebihara T, Kubota T. Effect of sulfidation atmosphere on the hydrodesulfurization activity of $SiO_2$-supported Co–Mo sulfide catalysts: local structure and intrinsic activity of the active sites. J Catal 2009;268:49–59.
[17] Li H, Duan X, Wu X, Zhuang X, Zhou H, Zhang Q, et al. Growth of alloy $MoS_{2x}Se_{2(1-x)}$ nanosheets with fully tunable chemical compositions and optical properties. J Am Chem Soc 2014;136:3756–9.
[18] Tongay S, Narang D, Kang J, Fan W, Ko C, Luce A, et al. Two-dimensional semiconductor alloys: monolayer $Mo_{1-x}W_xSe_2$. Appl Phys Lett 2014;104:012101.
[19] Zhang W, Li X, Jiang T, Song J, Lin Y, Zhu L, et al. CVD synthesis of $Mo_{(1-x)}W_xS_2$ and $MoS_{2(1-x)}Se_{2x}$ alloy monolayers aimed at tuning the bandgap of molybdenum disulfide. Nanoscale 2015;7:13554–60.
[20] Zou M, Chen J, Xiao L, Zhu H, Yang T, Zhang M, et al. $WSe_2$ and $W(Se_xS_{1-x})_2$ nanoflakes grown on carbon nanofibers for the electrocatalytic hydrogen evolution reaction. J Mater Chem A 2015;3:18090–7.
[21] Kiran V, Mukherjee D, Jenjeti R, Sampath S. Active guests in the $MoS_2$/$MoSe_2$ host lattice: efficient hydrogen evolution using few-layer alloys of $MoS_{2(1-x)}Se_{2x}$. Nanoscale 2014;6:12856–63.
[22] Lei Yang, Wang W, Fu Q, Zhang J, Xiang. $MoS_{2(1-x)}Se_{2x}$ nanobelts for enhanced hydrogen evolution. Electrochimica Acta 2015;185:236–41.
[23] Bougouma M, Batan A, Guel B, Segato T, Legma J, Reniers F, et al. Growth and characterization of large, high quality $MoSe_2$ single crystals. J Cryst Growth 2013;363:122–7.
[24] Abdallah W, Nelson A. Characterization of $MoSe_2$ (0001) and ion-sputtered $MoSe_2$ by XPS. J Mater Sci 2005;40:2679–81.
[25] Gong Y, Liu Z, Lupini A, Shi G, Lin J, Najmaei S, et al. Band gap engineering and layer-by-layer mapping of selenium-doped molybdenum disulfide. Nano Lett 2014;14:442–9.
[26] Kibsgaard J, Chen Z, Reinecke B, Jaramillo T. Engineering the surface structure of $MoS_2$ to preferentially expose active edge sites for electrocatalysis. Nat Mater 2012;11:963–9.
[27] Benoist L, Gonbeau D, Pfister-Guillouzo G, Schmidt E, Meunier G, Levasseur A. XPS analysis of lithium intercalation in thin films of molybdenum oxysulphides. Surf Interface Anal 1994;22:206–10.
[28] Wang H, Skeldon P, Thompson G. XPS studies of $MoS_2$ formed in associated with anodizing process. Surf Coat Technol 1997;91:200–7.
[29] Ueno T. Chemical shifts of photoelectron and Auger lines in Ag- or Cu-doped amorphous $GeSe_2$ and $As_2Se_3$. Jpn J Appl Phys 1983;22:1469.
[30] Yang C, Qin M, Wang Y, Wan D, Huang F, Lin J. Observation of an intermediate band in Sn-doped chalcopyrites with wide-spectrum solar response. Sci Rep 2013;3:1286.
[31] Wang G, Yang M, Li Z, Lin K, Jin Q, Xing C, et al. Synthesis and characterization of Zn-doped MgAl-layered double hydroxide nanoparticles as PVC heat stabilizer. J Nanopart Res 2013;15:1–8.
[32] Li Y, Wang H, Xie L, Liang Y, Hong G, Dai H. $MoS_2$ nanoparticles grown on graphene: an advanced catalyst for the hydrogen evolution reaction. J Am Chem Soc 2011;133:7296–9.
[33] Xie J, Zhang H, Li S, Wang R, Sun X, Zhou M, et al. Defect–rich $MoS_2$ ultrathin nanosheets with additional active edge sites for enhanced electrocatalytic hydrogen evolution. Adv Mater 2013;25:5807–13.
[34] Hinnemann B, Moses P, Bonde J, Jørgensen K, Nielsen J, Horch S, et al. Biomimetic hydrogen evolution: $MoS_2$ nanoparticles as catalyst for hydrogen evolution. J Am Chem Soc 2005;127:5308–9.
[35] Jaramillo T, Jørgensen K, Bonde J, Nielsen J, Horch S, Chorkendorff I. Identification of active edge sites for electrochemical $H_2$ evolution from $MoS_2$ nanocatalysts. Science 2007;317:100–2.

Please cite this article in press as: Yang H, et al., Synthesis of a $MoS_{2(1-x)}Se_{2x}$ ternary alloy on carbon nanofibers as the high efficient water splitting electrocatalyst, International Journal of Hydrogen Energy (2016), http://dx.doi.org/10.1016/j.ijhydene.2016.10.075